Journal of Mines, Metals and Fuels, *71(11): 1837-1857; 2023. DOI: 10.18311/jmmf/2023/35504*

Print ISSN : 0022-2755

Journal of Mines, Metals and Fuels

Contents available at: *www.informaticsjournals.com/index.php/jmmf*

Analysis and Optimization of Process Parameters of Powder Mixed Near Dry- EDM by using Grey Relational Optimization

Ajit and Sanjay Sundriyal*

School of Mechanical Engineering, Lingaya's Vidyapeeth, Faridabad - 121001, Haryana, India; ss95576@gmail.com

Abstract

The hybrid Electric Discharge Machine (PM-EDM) is the latest advancement in the removal of hard materials from workpieces while enhancing their performance and characteristics. This research project is focused on optimizing key process parameters, including material removal rate, tool wear, residual stresses, and surface finish. The approach utilized in this study involves employing the standard deviation-based objective weighting method in conjunction with GRA (Grey Relational Analysis) optimization to improve the hybrid PM-EDM process when applied to EN-31 material. Experimental runs were conducted to assess the impact of various input factors such as pulse on time, duty cycle, discharge current, and concentration of metallic powder. The GRA (Grey Relational Analysis)-based Taguchi method was employed for this purpose, and the experimental design followed an L-27 orthogonal array within the framework, facilitated by the use of minitab-20 software. A total of 27 experiments were conducted, encompassing diverse combinations of process parameters. Subsequently, an ANOVA (Analysis of Variance) was performed to scrutinize the impact of various inputs of discharge current, pulse on time, duty cycle, and powder concentration on MRR (Material Removal), TWR (Tool Wear), Ra (surface finish), and Rs (Residual stress).

Keywords: *Dry Air, EDM, Metallic Powder, MRR, Residual Stress, Surface Finish*

1.0 Introduction

Many researchers have been motivated to explore the use of a smaller quantity of lubrication in ND-EDM due to the imperative of reducing the environmental impact of cutting fluids used in machines ND-EDM involves machining with minimal amounts of lubricant or a mist applied directly to the work surface. This innovative approach was established as an alternative to the traditional coolant technique with high pressure, aiming to reduce the consumption of Metal-Working Fluids (MWFs) and subsequently lower their associated costs. In Near-Dry EDM (ND-EDM), the cooling medium consists of a mist of tiny droplets or aerosols made of a mixture of oil and air. In this context, mist refers to solid particles suspended in liquid or air. The EDM machine was the initial process to be provided, and the near-dry concept's efficiency was examined in 1981, leading to further investigations into using mist and various gases like argon and nitrogen as dielectric mixtures[1]. The study investigated the impact of introducing graphite powder into kerosene on the breakdown voltage in PM-EDM[2]. It was observed that certain concentrations of powder, such as graphite and silicon, when mixed with dielectric fluid resulted in the generation of exceptionally smooth surfaces due to the distribution of sparks in the gap of the spark[3]. Further, the

*Author for correspondence

properly adding metallic powders to the dielectric fluid led to an increase in MRR and a decrease in Tool Wear Rate (TWR). And an effort was developed to determine the prime output parameters for PM-EDM (Powder Mixed), and the research demonstrated that setting output results at their prime levels in PM-EDM resulted in a lower value of surface finish and a higher MRR[4]. Moreover, the study examined the effect of varying concentrations of powder (graphite) on output parameters, which are residual stress, tool wear rate, and material removal when the workpiece (H-11 die steel) is being machined. The results showed that adding 6 g/l of graphite powder improved material removal and finishing of the surface (Ra) while reducing tool wear (TWR)[5]. Another investigation involved different dielectrics in PM-EDM, and it demonstrated that HOPs study for analysis effectively decreased the cost of machining and dielectric destruction, as well as climate risks, in comparison to the traditional EDM machining method[6]. Further, the thermal aspects of PM-NDEDM were elucidated, and the study analyzed how changing individual process parameters influenced MRR, spanning from references[7-9]. Furthermore, in PMEDM, plasma channel features were optimised[10]. The study demonstrated that the plasma channel exhibited significantly greater stability in PM-EDM compared to plasma generated solely in pure kerosene oil. This enhanced stability resulted from the compression of the plasma within PM-EDM, thanks to the electric bridge formed by particles of conductive metallic powder in the oil of EDM. Furthermore, the research work on the workpiece of Titanium alloy (Ti-6Al-4V) was carried out to determine the characteristics of the workpiece during electrical discharge machining. The assessment focused on parameters such as tool wear and material removal rate. Additionally, the study examined the quality of the surface finish of machined workpiece, examining topographical features as well as surface morphology[11]. The consequence of silicon carbon powder concentration on surface topography, component deposition, and subsurface structures in the PMEDM of the material Ti-6Al-4V-ELI was an additional topic that was examined. The findings indicated that a higher concentration of suspended particles in dielectric fluid was promoted in the particulate form of a particle transfer mechanism[12]. The flushing or flooding mode helps to hold crucial functions in the operations of the electric discharge machine, and the improper flooding or flushing approach leads to irregular cutting and an unfavourable machining process[13]. An extensive investigation was also carried out in the realm of developing of residual stress on the machined samples. Efforts have been made to develop models aimed at minimizing these residual stresses[14]. It was investigated that the subsurface of the machined sample in EDM exhibited higher levels of residual stress compared to the top of the surface, primarily due to the high-up roughness on the top of the surface. In the context of wire EDM, a parametric investigation into residual stresses was carried out using the Taguchi optimization method to reduce stresses in aluminium jobs or workpieces[15]. Further, the stress in AISI H13 tool steel exposed to the EDM process was assessed using a mixture of the nano-indentation technique and the Raman spectroscopy method[16]. The residual stress produced on an object made of high-carbon, high-chromium D2 tool steel was specifically examined using the X-ray cosine method, which was used in a vibration-assisted hybrid EDM process for optimum residual stress[17]. And also performed the experiments for surface finish, tool wear rate, and MRR based on the comparative study between PMND-EDM and ND-EDM, non-conventional electrical discharge machining. As a result of the by PMND-EDM process, a lower tool wear rate was observed in the comparison of ND-EDM and non-conventional electrical discharge machining[18]. In the EDM process, SiC and Al powder in dielectric oil are utilized. It was noted that the working gap increases between workpiece and tool when there is an addition of metallic powder. Discrete sparks are generated due to the enlarged gap, which easily removes the material from the workpiece and therefore leads to a large finishing surface[19]. The adoption of a minimal-quantity lubrication system not only contributes to improved machining accuracy but also serves as a means to prevent environmental pollution and protect workers from hazards[20]. The utilization of optimal metal-working fluids not only leads to economic advantages but also promotes environmentally friendly machining practices. While prior research has touched upon PMND-EDM, it primarily focused on examining the Material Hardness (MH) of the machined component[21]. This study seeks to delve deeper into the intricacies of PMND-EDM. The Following an extensive review of existing literature, we have embarked on a comprehensive exploration of PMND-EDM, encompassing parameters

such as Material Removal (MRR), Tool Wear (TWR), surface roughness (Ra), and Residual Stress (RS). To facilitate this investigation, a novel experimental setup was devised, enabling the examination of the interplay between a three-phase dielectric, discharge current, pulse-on time, duty cycle, and metallic powder concentration. Specifically, our experimental setup was tailored to scrutinize how variations in metallic powder concentration impact machining performance with respect to the aforementioned factors. Finally, we conducted a comparative analysis of machining performance between ND-EDM and PMND-EDM, drawing insights from the experimental results. Many researchers work on the optimization of powder-mixed near-dry EDM process parameters. To our knowledge, no systematic studies have been carried out to integrate the standard deviation objective weighting method and the GRA-based Taguchi method for multi-objective optimization of the PMND-EDM process. Therefore, this study investigated the application of the standard deviation objective weighting method, which is an objective weighting technique, and the Grey Relational Analysis (GRA)-based Taguchi method to solve multiple criteria optimization problems in the powder-mixed ND-EDM process parameters of EN-31 die steel. The main objective of this work to improve mechanical characteristics like Material Removal (MRR), Tool Wear Rate (TWR), surface finish (Ra), and Residual stress (Rs) with consistent quality during powder-mixed ND-EDM by using Grey Relational Analysis.

2.0 Experimental Methods

2.1 Materials

We chose an EN-31 workpiece measuring 40 mm x 20 mm x 20 mm due to its exceptional hardness, impressive compressive strength, and resistance to abrasion. The remarkable wear resistance of this steel grade makes it an ideal choice for machining components. Moreover, EN-31 finds extensive use in the manufacturing industry. For the tool electrode, we opted for copper due to its superior thermal conductivity and other favorable characteristics for conducting experiments. You can find

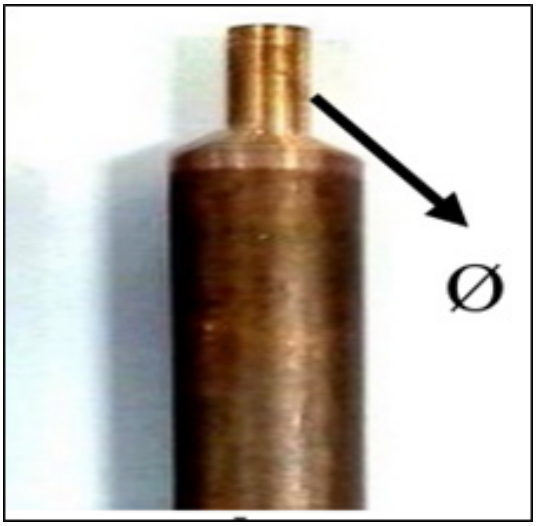

Figure 1. Copper tool.

Table 1. Chemical composition or structure and physical characteristics of the workpiece -EN-31 material[22-24]

Chemical properties		Physical properties	
ELEMENT	%	Thermal conductivity (W $m^{-1}K^{-1}$)	44.5
Carbon	0.90-1.20	Hardness(HRC)	63
Silicon	0.10-0.35	Yield stress (MPa)	450
Manganese	0.30-0.75	Tensile strength (MPa)	750
Sulphur	0.050	Density (kg m^{-3})	7850
Phosphorus	0.050	Melting point (^{0}C)	1540

the properties of the workpiece and tool in Table 1 and Table 2, respectively.

Table 2. Physical and chemical characteristics of the copper tool[22,25]

Properties	Values
Atomic number	29
Atomic weight	63.546
Density (Kg m^{-3})	8960
Melting point (^{O}C)	1083
Boiling point (^{O}C)	2567
Thermal conductivity (Wm $^{-1}$ K $^{-1}$)	385
Hardness (Mohs)	2.5-3
Tensile strength (MPa)	33.3
Bulk modulous (GPa)	140

2.1 Design of Experiment

In the present research, pulse on time, discharge current, powder concentration, and duty cycle were selected as input process parameters of the powder mixed near dry - EDM process. These input process parameters are at different levels, as shown in Table 3. Therefore, 81 (3 × 3 × 3 × 3) combinations were considered. However, according to the L-27 orthogonal array design, the samples could be developed or made in only 27 combinations and present outputs with the same reliability as if they were taken into account individually[26,27]. Employing the design of the experiment method in Minitab-19 software, orthogonal array design L-27, and the DOE (design of experiments), as shown in Table 4,

Table 3. Process parameters and their levels

Sr. No	PMNED-EDM process parameters	Level 1	Level 2	Level 3
1	Pulse on	50.00	275.00	500.00
2	Discharge Current	8.00	16.00	24.00
3	Duty Cycle	60.00	70.00	80.00
4	Powder Concentration	4.00	8.00	12.00

2.2 Powder mix EDM

The design and development of the latest and most advanced powder-mixed ND-EDM setup were successfully completed. Figure 2 illustrates the experimental

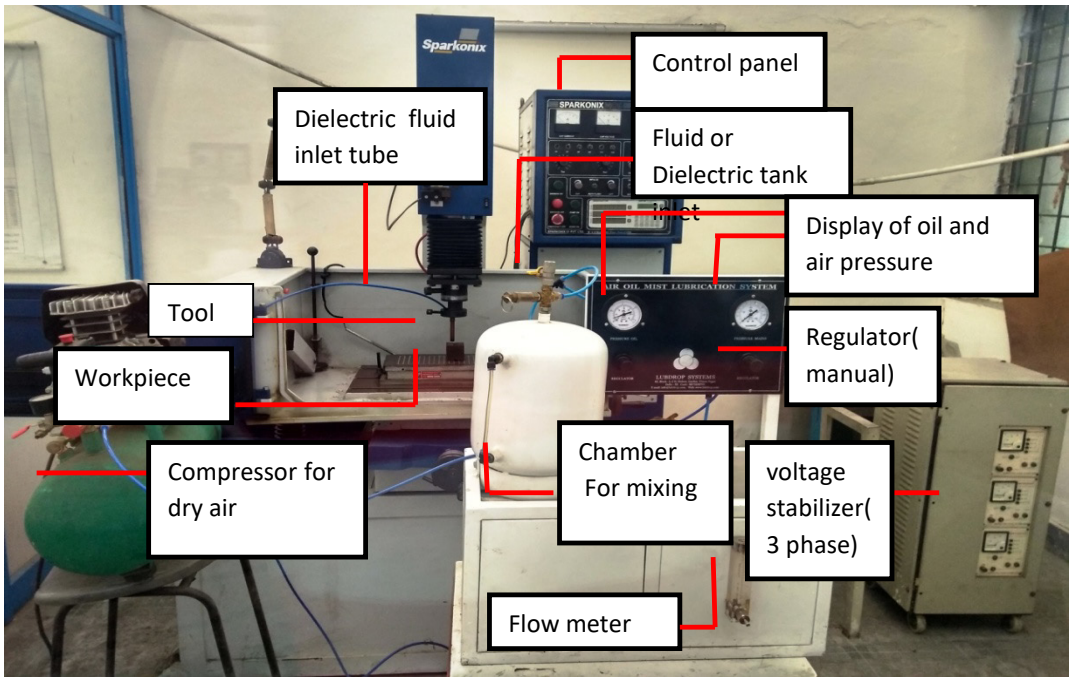

Figure 3. Experimental setup for powder-mixed ND-EDM.

Table 4. Specifications of the EDM Machine

Machine model	SPARKONIX 35-A
Max table speed (L x W)	420x280
X Travel	300 mm
Y Travel	200 mm
Z Travel	200 mm
Maximum job weight	300 Kg
Maximum job height	250 mm
Pump Motor	0.5 Hp
Dielectric tank	150 Litre
Input power supply	3 phase, 50 Hz and 640 V
Dielectric fluid	LL-221 kerosene based oil

Table 5. Classification by parameters

Parameters	Classification
Workpiece	EN-31 (40 mm × 20 mm × 20 mm)
Tool electrode	COPPER
Dielectric	Air + oil (LL-221) + metallic powder
Discharge current	8-24 A
Gap voltage	25 V
Pulse on / off	500 µs/ 50 µs
Polarity	+ve
Powder concentration	4 g/l, 8 g/l, 12 g/l
Flow meter of dielectric	0 ml/min to 20 ml/min
Air and oil pressure	0.6 MPa
Powder material	Zinc (22 µm)
Stabilizing agent	Glycerol (5 %)

arrangement for PMND-EDM, which was crafted with minimal resource input, prioritizing environmental friendliness while achieving the characteristics of the required response. This innovative PMND-EDM setup employs a heterogeneous mixture comprising three phases-solid, liquid, and gas-as its medium of dielectric. The setup's panel incorporates various key components,

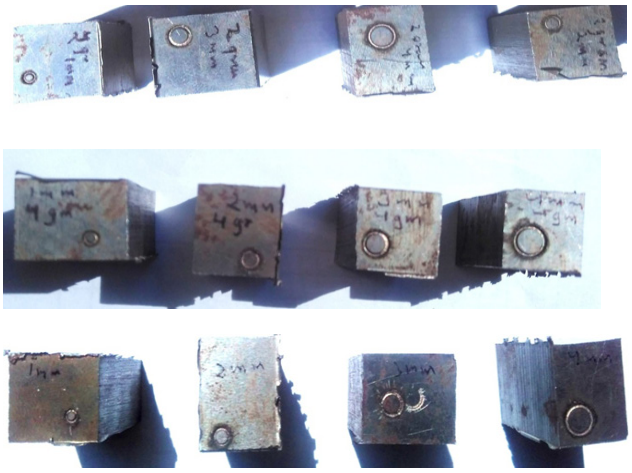

Figure 3. Machined samples (PMND-EDM).

including a dielectric chamber for mixing, mist flow meter for a dielectric, manual regulators, and pressure gauges that play a crucial role in determining the working pressure of the dielectric medium. After that, the material removal rate is calculated according to Sundriyal s. discussed in literature survey[22,28].

2.3 Standard deviation objective weighting Method

The standard deviation objective weighting method was employed for evaluating each criteria's weight (w_j). Based on the weight of responses, the Performance Defining Criteria (PDC) were decided for all responses[29]. First, an initial decision matrix (9 experiments and five process parameters) is defined. Then after calculating the best and worst values for all process parameters, the decision matrix is normalized using Equation 1.

$$X_{ij}^{+} = \frac{X_{ij} - X_j^{\text{worst}}}{X_j^{\text{best}} - X_j^{\text{worst}}} \quad (1)$$

where X_{ij}^{+} represents the normalized value of the ith design on the jth response. By applying correlation and standard deviation coefficient (Minitab 19 software). After this, correlation and standard deviation coefficients were employed to evaluate information creation. Then, each criterion's weight (ξ_j) was calculated using Equation 2[30.31]. Based on the weight of responses, the Performance-Defining Criteria (PDC) was decided for all responses, as shown in Table 6.

Table 6. Performance Defining Criteria (PDCs)

SN	Performance-Defining Criteria (PDC)			Impact on PDC
	Response	Weight ξ_j	Designation	
1	Material removal rate	0.7	PDC-1	Higher the better
2	Tool wear rate	0.1	PDC-2	Lower the better
3	Surface finish	0.1	PDC-3	Lower the better
4	Residual stress	0.1	PDC-4	Lower the better

$$\xi_j = \frac{c_j}{\sum_{k=1}^{m} c_j} \quad (2)$$

Where, $\xi_j \geq 0$ and $\sum_{k=1}^{m} c_j = 1$

3.0 Hybrid Gray Relational Methodology

3.1 S/N ratio

Based on characteristics, three SN (Signal to Noise) ratios are available, mainly lower the better, higher the better, and nominal the better. In this research, higher values are used for rate of material removal, rate of tool wear, surface roughness, and residual stress. The expressions representing these approaches are listed below:

SN ratio for "larger is better"

$$SN_L = -10log(\frac{1}{n}\sum_{i=1}^{n}\frac{1}{y^{i^2}} \quad (3)$$

SNs ratio for "Smaller is better"

$$SN_s = -10log\sum_{i=1}^{n} y^{i^2} \quad (4)$$

SNn ratio for "nominal is better"

$$SN_n = 10\log 10\ (Square of\ mean / variance) \quad (5)$$

3.2 Normalisation of S/N Ratio

For larger the better for material removal, tool wear, surface finish and residual stress.

$$y_i^*(m) = \frac{y_i(m) - \min y_i(m)}{\max y_i(m) - \min y_i(m)} \quad (6)$$

For smaller, the better

$$y_i^*(m) = \frac{\max y_i(m) - y_i(m)}{\max y_i(m) - \min y_i(m)}. \quad (7)$$

For nominal, the better for

$$y_i^*(m) = \frac{1 - / y_i(m) - y_0 b(m) /}{\max y_i(m) - y_0 b(m)}. \quad (8)$$

Y∗(m) and yi(m) are the data preprocessing and comparability arrangements. m = 1, m = 2, m = 3, m = 4 for material removal (MRR), Tool Wear (TWR), surface finish (Ra), and residual stress (Rs), i = 1, 2, 3, 27 for experiment no. 1 to 27.

3.3 Deviation Sequence

The deviation sequence can be represented as31:

$$\Delta_{0i}(k) = \left| y_0^*(m) - y_k^*(m) \right| \quad (9)$$

3.4 Grey Relational Coefficient (GRC)

The connection among best with real normalized experimental value is expressed by GRC[32].

$$GRC = \xi_i(k) = \frac{\Delta_{\min} + \xi\Delta_{\max}}{\Delta_{0i}(k) + \xi\Delta_{\max}} \quad (10)$$

3.5 Grey Relational Grade

It is determined by averaging the GRCs for every performance property. The overall calculation of multiple performance characteristics depends on grey relational grades[32].

$$\gamma_i = \frac{1}{n}\sum_{k=1}^{n}\xi_i(k) \qquad (11)$$

4.0 Optimization using GRA Method

The experiments were conducted at room temperature as per the face-centered composite. MRR was calculated from load-displacement graphs for MRR, TWR, surface finish (Ra), and residual stress (Rs) recorded for all 27 runs of the experiment, as shown in Figures 4-7.

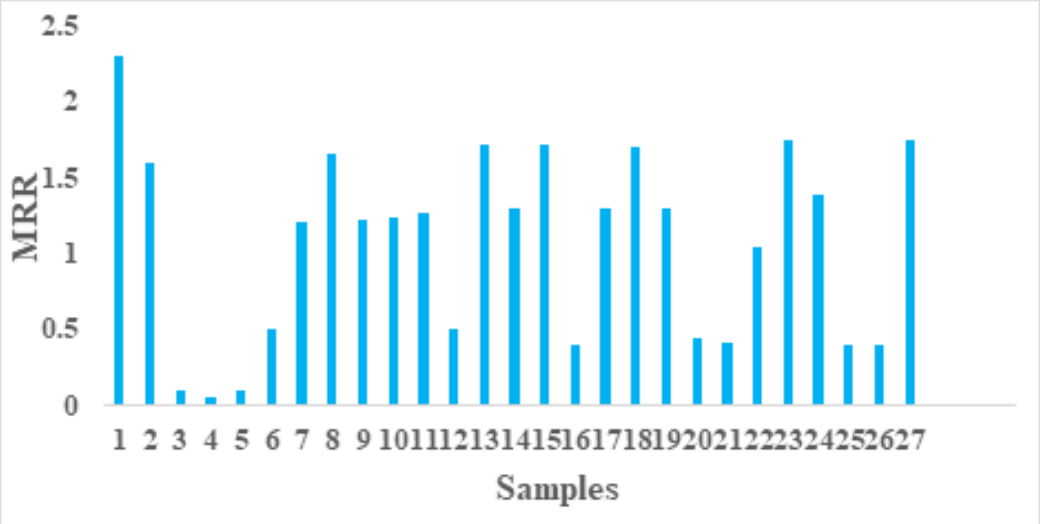

Figure 4. Load-Displacement plot for all experiments.

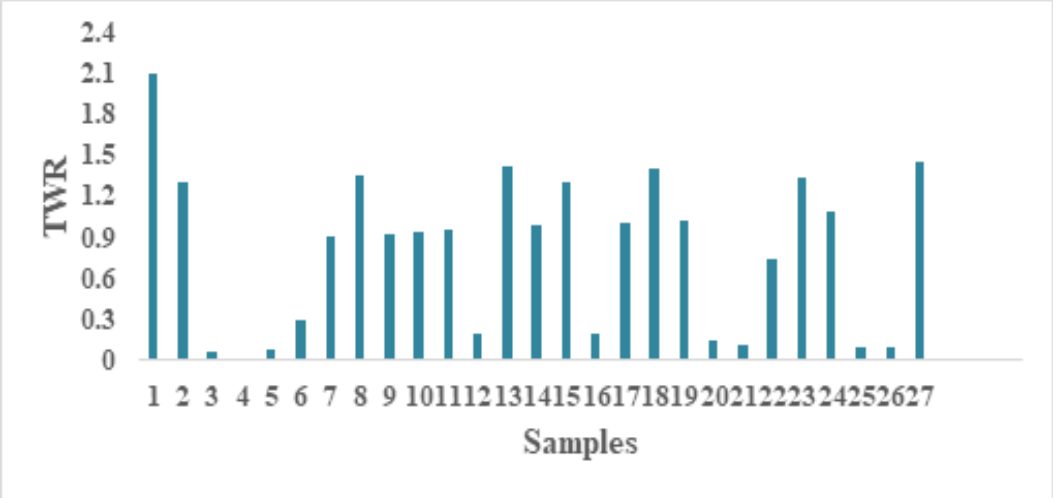

Figure 5. Tool wear rate for samples 1-27.

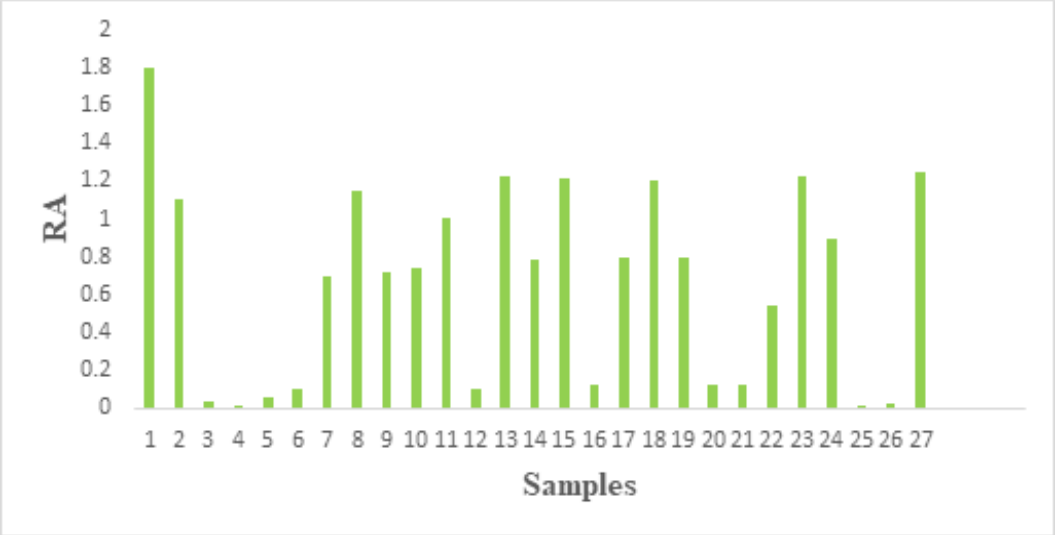

Figure 6. Surface finish for samples 1-27.

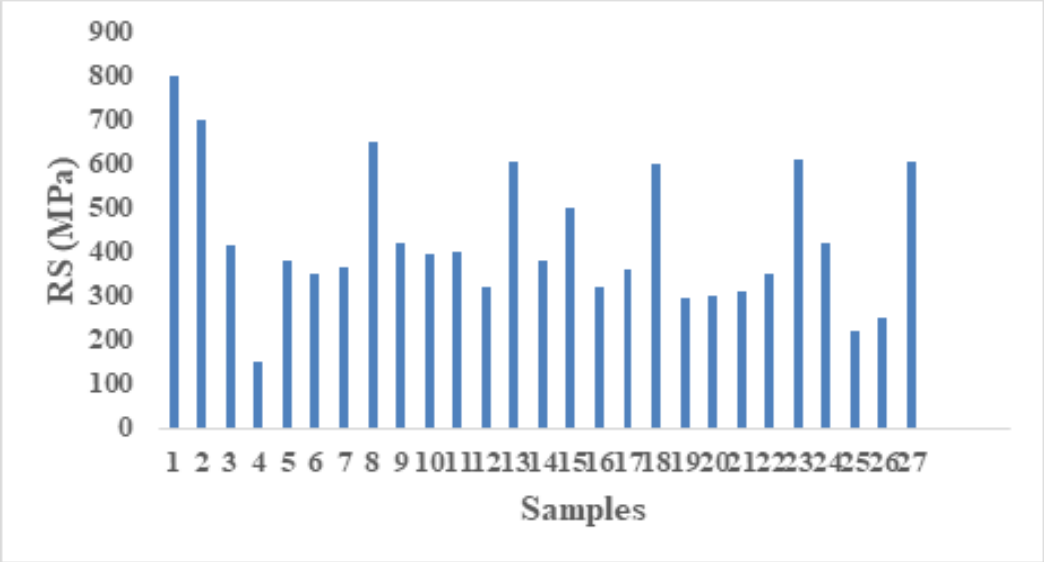

Figure 7. Residual stress for samples 1-27.

The S/N ratio was calculated using Equation 3 for MRR, TWR, and Ra, as shown in Table 8. The normalised S/N ratio was calculated using Equation 6 for Material Removal (MRR), Tool Wear (TWR), surface finish (Ra), and residual stress (Rs) which is shown in Table 9. The deviation sequence was computed using equation 9 for all experimental trials and is shown in Table 10.

Grey Relational Coefficient (GRC) was calculated by using Equation 10. The weight of each response (is taken from Table 10, which is evaluated using the Standard deviation objective weighting method and shown in Table 1031. Grey Relational Grade (GRG) and ranking were calculated using Equation 11 and shown in Table 12.

As shown in Figure 9(a), it shows the effect of discharge current, pulse on, duty cycle, and powder concentration on material removal. It is seen that as the duty cycle increases, the pulse on time and discharge current increase. If the discharge current increases, the material

Table 7. Experiment results

	Factor-1	Factor-2	Factor-3	Factor-4	MRR	TWR	RA	RS
	A: Pulse on	B: Discharge Current	C: Duty Cycle	D: Powder Concentration				
	µs	Ampere	%	g/l	mg/min	mm^3/min	µm	MPa
1	50	8	60	4	1.6	1.3	1.1	700
2	50	8	60	4	0.09	0.06	0.04	415
3	50	8	60	4	0.05	0.02	0.01	150
4	50	16	70	8	0.1	0.08	0.06	380
5	50	16	70	8	0.5	0.3	0.1	350
6	50	16	70	8	1.2	0.9	0.7	366
7	50	24	80	12	1.65	1.35	1.15	650
8	50	24	80	12	1.22	0.92	0.72	420
9	50	24	80	12	1.24	0.94	0.74	395
10	275	8	70	12	1.26	0.96	1.01	398
11	275	8	70	12	0.5	0.2	0.1	320
12	275	8	70	12	1.72	1.42	1.22	605
13	275	16	80	4	1.29	0.99	0.79	380
14	275	16	80	4	1.71	1.31	1.21	500
15	275	16	80	4	0.39	0.19	0.12	320
16	275	24	60	8	1.3	1	0.8	360
17	275	24	60	8	1.7	1.4	1.2	600
18	275	24	60	8	1.3	1.02	0.8	295
19	500	8	80	8	0.44	0.14	0.12	300
20	500	8	80	8	0.41	0.11	0.12	309
21	500	8	80	8	1.04	0.74	0.54	349
22	500	16	60	12	1.74	1.34	1.22	610
23	500	16	60	12	1.39	1.09	0.89	419
24	500	16	60	12	0.4	0.1	0.011	220
25	500	24	70	4	0.39	0.09	0.03	251
26	500	24	70	4	1.75	1.45	1.25	605
27	500	24	70	4	2.3	2.1	1.8	800

Table 8. S/N ratio

	Factor 1	Factor 2	Factor 3	Factor 4	S/N Ratio MRR	S/N Ratio TWR	S/N Ratio RA	S/N Ratio RS
Run	**A: Pulse on**	**B: Discharge Current**	**C: Duty Cycle**	**D: Powder Concentration**				
	µs	Ampere	%	g/l				
1	50	8	60	4	7.234557	-6.44439	-5.10545	-58.0618
2	50	8	60	4	4.0824	-2.27887	-0.82785	-56.90196
3	50	8	60	4	-20.9151	24.43697	27.9588	-52.36096
4	50	16	70	8	-26.0206	33.9794	40	-43.52183
5	50	16	70	8	-20	21.9382	24.43697	-51.59567
6	50	16	70	8	-6.0206	10.45757	20	-50.88136
7	50	24	80	12	1.583625	0.91515	3.098039	-51.26962
8	50	24	80	12	4.349679	-2.60668	-1.21396	-56.25827
9	50	24	80	12	1.727197	0.724243	2.85335	-52.46499
10	275	8	70	12	1.868434	0.537443	2.615366	-51.93194
11	275	8	70	12	2.007411	0.354575	-0.08643	-51.99766
12	275	8	70	12	-6.0206	13.9794	20	-50.103
13	275	16	80	4	4.710569	-3.04577	-1.7272	-55.63511
14	275	16	80	4	2.211794	0.087296	2.047458	-51.59567
15	275	16	80	4	4.659922	-2.34543	-1.65571	-53.9794
16	275	24	60	8	-8.17871	14.42493	18.41638	-50.103
17	275	24	60	8	2.278867	0	1.9382	-51.12605
18	275	24	60	8	4.608978	-2.92256	-1.58362	-55.56303
19	500	8	80	8	2.278867	-0.172	1.9382	-49.39644
20	500	8	80	8	-7.13095	17.07744	18.41638	-49.54243
21	500	8	80	8	-7.74432	19.17215	18.41638	-49.79917
22	500	16	60	12	0.340667	2.615366	5.352125	-50.85651
23	500	16	60	12	4.810985	-2.5421	-1.7272	-55.7066
24	500	16	60	12	2.860296	-0.74853	1.0122	-52.44428
25	500	24	70	4	-7.9588	20	39.17215	-46.84845
26	500	24	70	4	-8.17871	20.91515	30.45757	-47.99347
27	500	24	70	4	4.860761	-3.22736	-1.9382	-55.63511

Table 9. Normalise signal-to-noise ratio of response

	Factor-1	Factor-2	Factor-3	Factor-4	MRR	TWR	RA	RS
Run	A: Pulse on	B: Discharge Current	C: Duty Cycle	D: Powder Concen-tration				
	µs	Ampere	%	g/l				
1	50	8	60	4	1	1	1	1
2	50	8	60	4	0.905213	0.896954	0.905165	0.920231
3	50	8	60	4	0.153524	0.23606	0.266957	0.6079197
4	50	16	70	8	0	0	0	0
5	50	16	70	8	0.181043	0.297874	0.345036	0.5552862
6	50	16	70	8	0.60141	0.581881	0.443405	0.5061588
7	50	24	80	12	0.830074	0.81794	0.818126	0.5328618
8	50	24	80	12	0.91325	0.905063	0.913725	0.8759604
9	50	24	80	12	0.834391	0.822663	0.823551	0.615074
10	275	8	70	12	0.838638	0.827284	0.828827	0.5784134
11	275	8	70	12	0.842817	0.831808	0.888727	0.5829334
12	275	8	70	12	0.60141	0.494758	0.443405	0.4526263
13	275	16	80	4	0.924102	0.915925	0.925103	0.833102
14	275	16	80	4	0.848963	0.83842	0.841418	0.5552862
15	275	16	80	4	0.922579	0.8986	0.923518	0.7192292
16	275	24	60	8	0.536515	0.483737	0.478515	0.4526263
17	275	24	60	8	0.85098	0.840579	0.84384	0.5229875
18	275	24	60	8	0.921047	0.912877	0.92192	0.8281445
19	500	8	80	8	0.85098	0.844834	0.84384	0.404032
20	500	8	80	8	0.568022	0.418119	0.478515	0.4140722
21	500	8	80	8	0.549577	0.366301	0.478515	0.4317301
22	500	16	60	12	0.792697	0.775881	0.768153	0.5044495
23	500	16	60	12	0.927122	0.903466	0.925103	0.8380188
24	500	16	60	12	0.868464	0.859096	0.86437	0.61365
25	500	24	70	4	0.543128	0.345821	0.018354	0.2287919
26	500	24	70	4	0.536515	0.323182	0.211558	0.3075418
27	500	24	70	4	0.928619	0.920418	0.929781	0.833102

Table 10. The deviation Sequences for all experiments

Run	$\Delta_{0i}(1)$	$\Delta_{0i}(2)$	$\Delta_{0i}(3)$	$\Delta_{0i}(4)$
1	0	0	0	0
2	0.094787	0.103046	0.094835	0.079769
3	0.846476	0.76394	0.733043	0.3920803
4	1	1	1	1
5	0.818957	0.702126	0.654964	0.4447138
6	0.39859	0.418119	0.556595	0.4938412
7	0.169926	0.18206	0.181874	0.4671382
8	0.08675	0.094937	0.086275	0.1240396
9	0.165609	0.177337	0.176449	0.384926
10	0.161362	0.172716	0.171173	0.4215866
11	0.157183	0.168192	0.111273	0.4170666
12	0.39859	0.505242	0.556595	0.5473737
13	0.075898	0.084075	0.074897	0.166898
14	0.151037	0.16158	0.158582	0.4447138
15	0.077421	0.1014	0.076482	0.2807708
16	0.463485	0.516263	0.521485	0.5473737
17	0.14902	0.159421	0.15616	0.4770125
18	0.078953	0.087123	0.07808	0.1718555
19	0.14902	0.155166	0.15616	0.595968
20	0.431978	0.581881	0.521485	0.5859278
21	0.450423	0.633699	0.521485	0.5682699
22	0.207303	0.224119	0.231847	0.4955505
23	0.072878	0.096534	0.074897	0.1619812
24	0.131536	0.140904	0.13563	0.38635
25	0.456872	0.654179	0.981646	0.7712081
26	0.463485	0.676818	0.788442	0.6924582
27	0.071381	0.079582	0.070219	0.166898
ξ	0.7	0.1	0.1	0.1

Table 11. Grey Relational Coefficient for the response

Run	$\Delta_{0i}(1)$	$\Delta_{0i}(2)$	$\Delta_{0i}(3)$	$\Delta_{0i}(4)$
1	1	1	1	1
2	0.880739	0.492499	0.513254	0.5562695
3	0.452642	0.115749	0.120042	0.2032189
4	0.411765	0.090909	0.090909	0.0909091
5	0.460842	0.124669	0.132457	0.1835826
6	0.637181	0.193006	0.152301	0.1683952
7	0.804666	0.354535	0.354769	0.1763239
8	0.889736	0.512986	0.536839	0.4463497
9	0.808679	0.360572	0.361731	0.206217
10	0.812666	0.366682	0.368769	0.1917227
11	0.816628	0.372867	0.473321	0.1933987
12	0.637181	0.165223	0.152301	0.1544703
13	0.902181	0.543258	0.571766	0.374675
14	0.822526	0.382292	0.386725	0.1835826
15	0.900413	0.496525	0.566631	0.2626252
16	0.601641	0.162268	0.160905	0.1544703
17	0.82448	0.385474	0.390382	0.1733065
18	0.898643	0.534409	0.561546	0.3678425
19	0.82448	0.391902	0.390382	0.1436848
20	0.618386	0.146653	0.160905	0.1457879
21	0.608472	0.136296	0.160905	0.1496401
22	0.771517	0.308528	0.301343	0.1679119
23	0.905706	0.508817	0.571766	0.3817067
24	0.841815	0.415104	0.424394	0.2056132
25	0.60508	0.132595	0.092452	0.1147831
26	0.601641	0.12873	0.112557	0.1261896
27	0.907463	0.556847	0.587479	0.374675

Table 12. Grey Relational Grade and its order

	Factor 1	Factor 2	Factor 3	Factor 4	GRG	Rank
Run	**A: Pulse on**	**B: Discharge Current**	**C: Duty Cycle**	**D: Powder Concentration**		
	µs	Ampere	%	g/l		
1	50	8	60	4	1	**1**
2	50	8	60	4	0.61069	**2**
3	50	8	60	4	0.222913	**26**
4	50	16	70	8	0.171123	**27**
5	50	16	70	8	0.225388	**25**
6	50	16	70	8	0.287721	**18**
7	50	24	80	12	0.422573	**16**
8	50	24	80	12	0.596478	**5**
9	50	24	80	12	0.4343	**15**
10	275	8	70	12	0.43496	**14**
11	275	8	70	12	0.464054	**10**
12	275	8	70	12	0.277294	**19**
13	275	16	80	4	0.59797	**4**
14	275	16	80	4	0.443781	**11**
15	275	16	80	4	0.556549	8
16	275	24	60	8	0.269821	**20**
17	275	24	60	8	0.443411	**12**
18	275	24	60	8	0.59061	**7**
19	500	8	80	8	0.437612	**13**
20	500	8	80	8	0.267933	**21**
21	500	8	80	8	0.263828	**22**
22	500	16	60	12	0.387325	**17**
23	500	16	60	12	0.591999	**6**
24	500	16	60	12	0.471732	**9**
25	500	24	70	4	0.236227	**24**
26	500	24	70	4	0.242279	**23**
27	500	24	70	4	0.606616	**3**

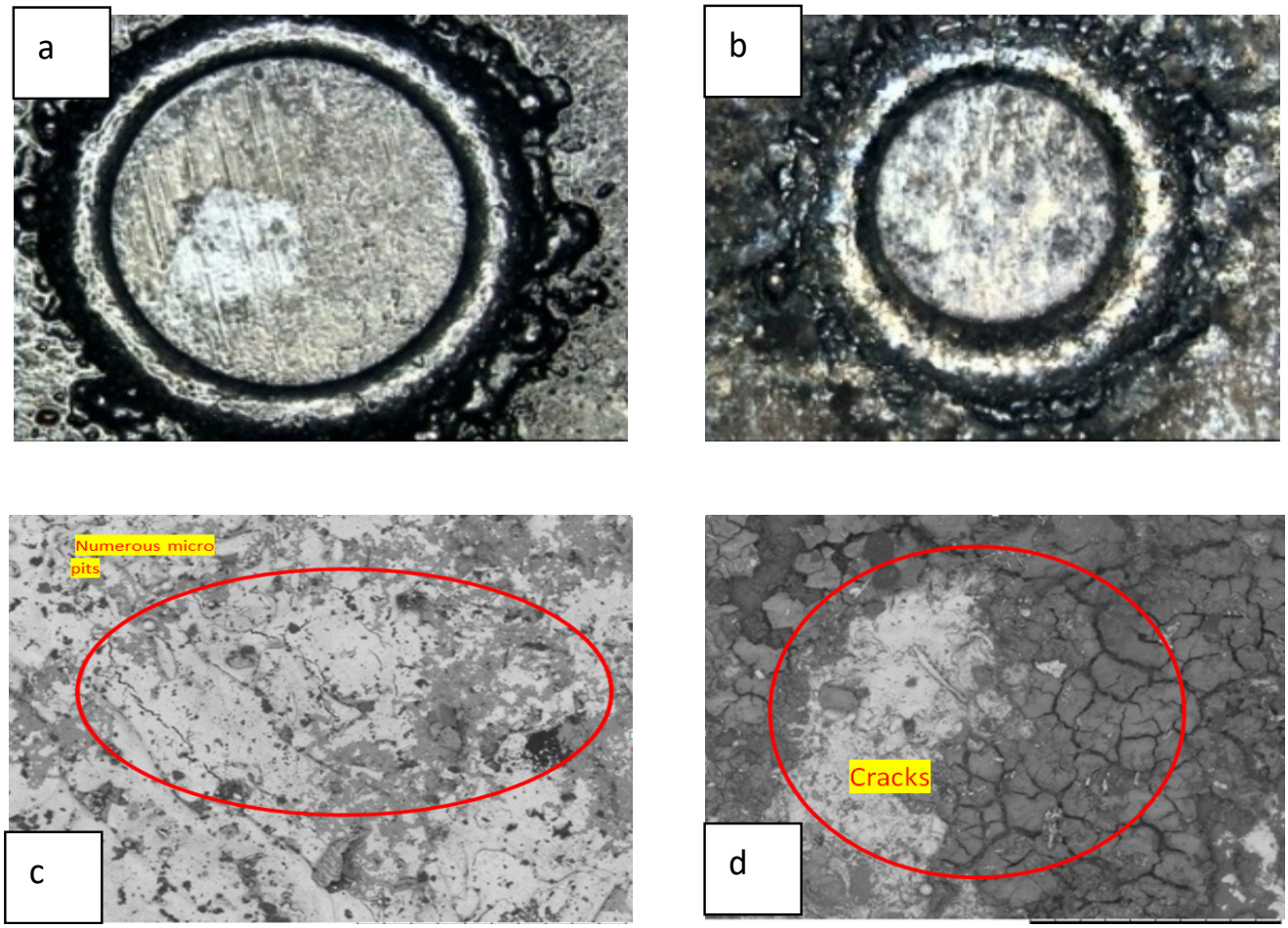

Figure 8. Figure 8(a). Machined sample for PMND-EDM. (b). Machined sample for ND-EDM. (c). SEM image of the machined area in PMND-EDM. (d). SEM image of the machined area in near-dry EDM.

removal rate increases due to discharge energy and spark intensity, leading to more material removal. In the context of PMND-EDM, the introduction of metallic powder and the addition of a liquid to compressed air reduce the dielectric insulating medium's strength between the workpiece electrodes and the tool. Consequently, this enhances ionization effects and discharge conditions[21]. It is stimulating that adding a little powder to EDM increases the dielectric strength of the electric field and affects when the discharge occurs. This leads to the observation that a higher MRR can be achieved with specific parameters: a pulse of 275 µs, a discharge current of 8A, a duty cycle of 60%, and a concentration of metallic powder of 4 g/l in PMND-EDM. Experimental evidence confirms that PMND-EDM results in a significant 17.85% increase in MRR compared to ND-EDM[22]. You can view the samples of workpieces machined using PMND-EDM and near-dry EDM in Figure 8 (a, b). And 8(c,d) show the SEM images of machined surfaces. It can be seen that the large craters and cracks show up in ND-EDM as compared to PMND-EDM[23].

Results from experiments have shown that PMND-EDM has a much higher Material Removal Rate (MRR) than regular near-dry EDM. This improvement happened because metallic powder was added to the dielectric oil. This lowers the electrical density and makes the spark gap bigger. Consequently, the resulting sparks are distributed more evenly across the machined surface (as referenced in[24]). Furthermore, this study observed that the expanded spark gap facilitated more efficient debris

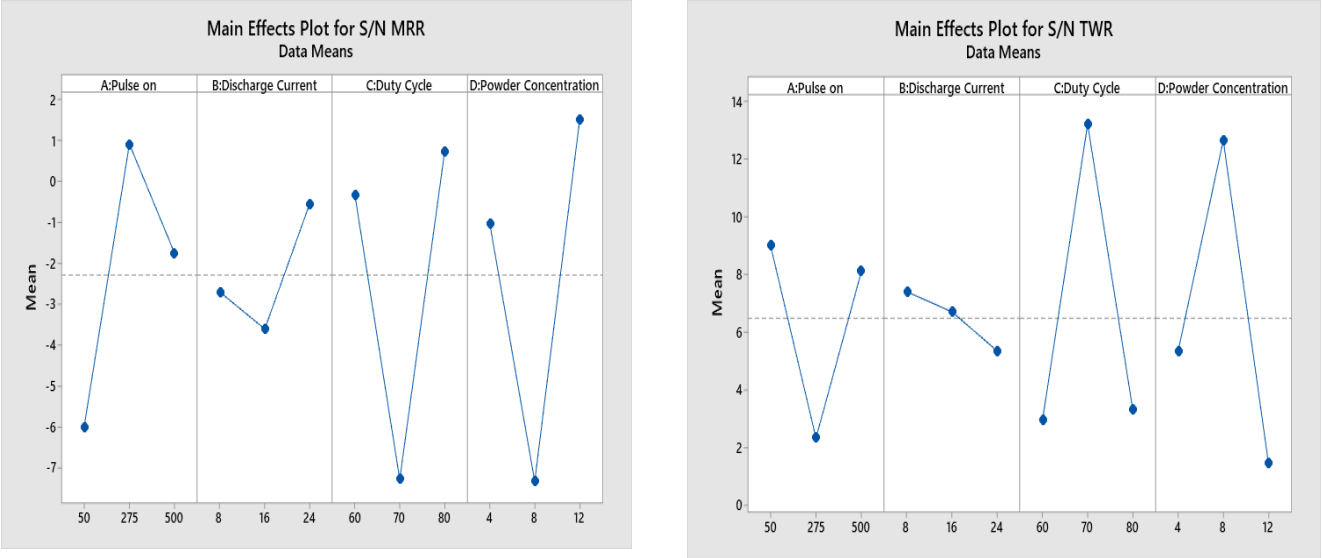

Figure 9. (a). Main effects plot for MRR. (b). Main effects plot for TWR.

removal during machining, resulting in a higher-quality surface finish for the machined products (as noted in[25]). Notably, the concentration powder played a crucial role in influencing the spark gap. For instance, when the powder concentration was maintained at 4 g/l, the plasma channel remained small, leading to the formation of intense craters on the workpiece[26,27]. If the discharge current and pulse on increased, a higher erosion rate was achieved. From Figure 9(b), which shows the effect of input parameters on Tool Wear Rate (TWR), it can be seen that a lower value of tool wear rate was observed when the mist of powder concentration increased on duty cycle, the pulse on time, and discharge current increased due to this. The tool's strong thermal conductivity and the workpiece materials low specific heat make for more effective TWR findings[11,28]. It was observed that the lower the tool wear rate in PM-EDM as compared to ND-EDM at input parameters of 4 g/l powder concentration, a pulse

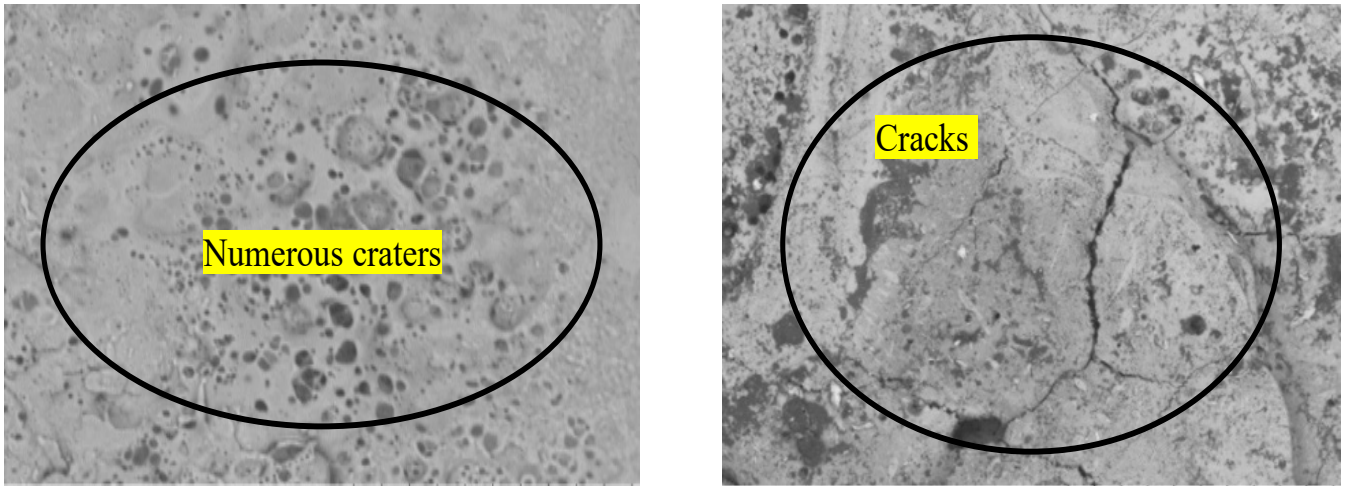

Figure 10. **(a).** EN -31 Sample machined by PMND-EDM. **(b)**. EN -31 Sample machined by ND-EDM.

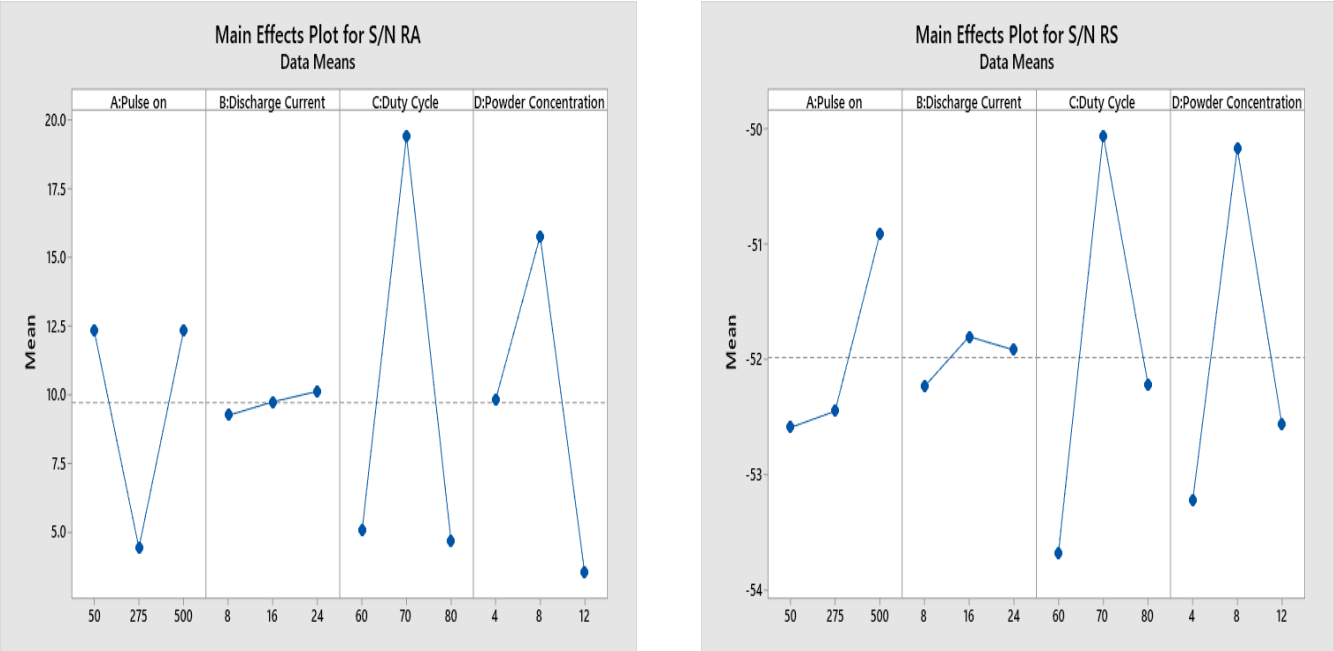

Figure 11. **(a).** Main effects plot for Surface Finish. **(b).** Main effects plot for Residual Stress.

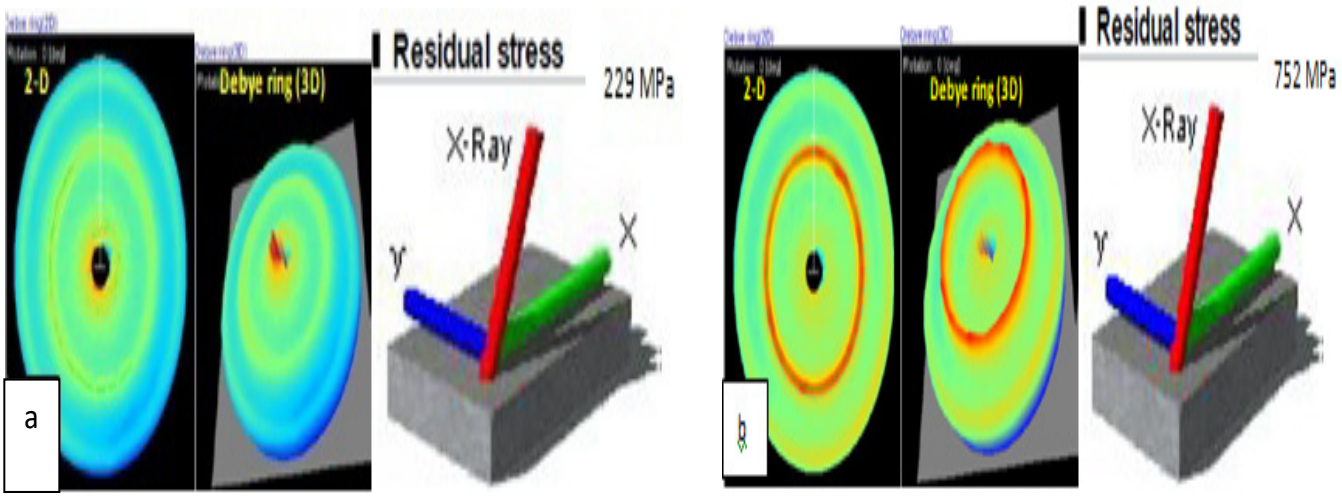

Figure 12. **(a).** Debye Scherer rings with residual stress values of machined EN-31 samples PMND-EDM. **(b).** Debye Scherer rings with residual stress values of machined EN-31 samples by ND-EDM.

on of 275 μs, a discharge current of 8A, and a duty cycle of 60% .

From Figure 11(a), which shows the effect of various inputs on surface roughness, it can be seen that when there are increases in discharge current, duty cycle, and pulse on time, a better surface of finish is achieved. The metallic powder played a major role in changing the spark gap, which improved surface quality[28,29]. Due to the lack of metallic powder, a maximum increase in surface quality of 16.36% was seen when comparing PMND-EDM to near-dry EDM. As can be seen in Figures 10(a,b), this results in the appearance of a large machined area

Table 13. Responses for the GRA grade

Sr. No	PMNED-EDM process parameters	Grey relational grade			Main effect (Max-Min)	Rank	Mean
		Level 1	Level 2	Level 3			
1	Pulse on	0.4412	**0.4531**	0.3895	0.0636	2	0.427933
2	Discharge Current	**0.4870**	0.4261	0.3706	0.1164	1	0.4279
3	Duty Cycle	**0.4508**	0.4174	0.4142	0.0366	4	0.427467
4	Powder Concentration	**0.4590**	0.4110	0.4124	0.048	3	0.427467

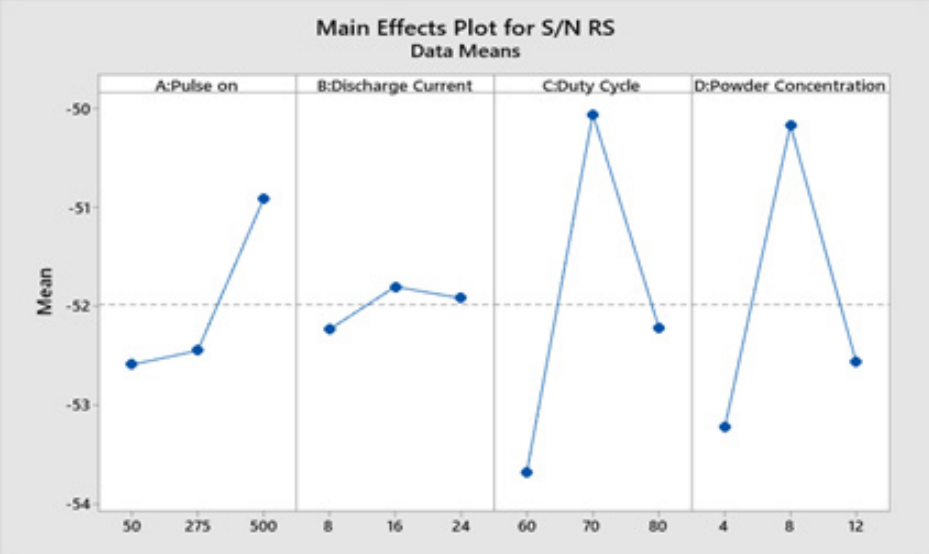

Figure 13. Main effects plot for GRG.

with imperfections and cracks. The metallic powder was an important factor in influencing the spark gap, which led to an improvement in surface quality. The maximum percentage increase in surface finish was 16.36% in PMND-EDM as compared to near-dry EDM[30,31]. It was observed due to the absence of metallic powder. This leads to the formation of a large machined area with an uneven surface with cracks, as shown in Figure 10(b).

The graph 11(b) shows the impact of different input parameters on the residual stress. It is clear that a pulse duration of 275 s, a discharge current of 8 A, a duty cycle of 60%, and a powder concentration of 4 g/l are the best variables for achieving the lowest residual stress values. The images 12(a,b) shows the lower value of residual stress for PM-EDM as compared to ND-EDM[24]. Comparing these results to the stresses found in pieces machined with ND-EDM, smaller residual stresses are produced. Based on Bragg's rule, residual stress was measured using X-ray analysis, with an X-ray session lasting 30 seconds. With a sample distance of 39 mm and an X-ray incidence angle of 35 degrees, the X-ray tube is operated at 1 mA and 30 kV. Every measurement was performed with an X-ray wavelength of 2.29 A, and at a temperature of 26 degrees Celsius, all measurements were taken. The distribution of residual stress across the machined surface is represented by a debye ring. The yellow region designates a zone of relatively lower stress created on the surface that was machined, while the red ring indicates the area of

maximal stress intensity. The area with the least amount of induced stress is shown as the blue zone, in contrast. The reduction in residual stresses shown in PMND-EDM can be attributed to improved flushing conditions and the even distribution of heat or energy plasma all over the machined surface, which relieves some of the residual tensions on the surface[25,32].

The mean of the GRC for the pulse frequency at stages 1, 2, and 3 was evaluated by the averaged GRC for experiments 1 to 9, 10 to 18, and 19 to 27 and given in Table 13, which shows the responses for the GRA grade. The importance level of each factor for the grey relational grade is determined by the rank of the process parameters (discharge current > pulse on > powder concentration > duty cycle). This means that pulse frequency plays a dominant role in the overall performance of laser welding. Figure 13 shows the GRG's main effects plot, which was taken from Minitab 19. It can be seen that the optimal process parameters were A2B1C1D1 with a pulse of 275 µs, a discharge current of 8A, a duty cycle of 60%, and a powder concentration of 4 g/l.

5.0 Conclusion

The excellent performance of output on EN-31 die steel is achieved by using a powder-mixed, near-dry EDM. Powder-mixed near-dry EDM has been successfully performed based on the orthogonal array design of experiments on selected materials. This work uses the standard deviation objective weighting method - grey relational optimization method to improve multi-responses such as material removal, tool wear rate, surface finish, and residual stress by using powder mixed-EDM as a comparison of ND-EDM. It is found that the optimum parameter combination **A2B1C1D1** is preferred. The optimum process parameters obtained for the powder mixed near dry EDM are a pulse off 275 µs(A2), a discharge current of 8 A(B1), a duty cycle of 60%(C1), and a powder concentration of 4 g/l(D1). The pulse plays a significant role in PMND-EDM, followed by discharge current, duty cycle, and powder concentration. The standard deviation objective weighting method efficiently estimated the weight fractions for material removal, tool wear, surface roughness, and residual stress, which were 0.7, 0.1, 0.1, and 0.1, respectively.

6.0 References

1. Tanimura T. Development of EDM in the Mist. Proceedings of Ninth International Symposium of Electro Machining. 1989; 313-6.
2. Jeswani ML. Effect of the addition of graphite powder to kerosene used as the dielectric fluid in electrical discharge machining. Wear. 1981; 70(2):133-9. https://doi.org/10.1016/0043-1648(81)90148-4
3. Wong YS, Lim LC, Rahuman I, Tee WM. The near-mirror-finish phenomenon in EDM using powder-mixed dielectric. Journal of Materials Processing Technology. 1998; 79(1-3):30-40. https://doi.org/10.1016/S0924-0136(97)00450-0
4. Kansal HK, Singh S, Kumar P. Parametric optimization of powder mixed electrical discharge machining by response surface methodology. Journal of Materials Processing Technology. 2005; 169(3):427-36. https://doi.org/10.1016/j.jmatprotec.2005.03.028
5. Tripathy S, Tripathy DK. Optimization of process parameters and investigation on surface characteristics during EDM and powder-mixed EDM. In Innovative Design and Development Practices in Aerospace and Automotive Engineering: I-DAD. Springer Singapore. 2016; 385-91. https://doi.org/10.1007/978-981-10-1771-1_41
6. Singh J, Sharma RK. Assessing the effects of different dielectrics on environmentally conscious powder-mixed EDM of difficult-to-machine material (WC-Co). Frontiers of Mechanical Engineering. 2016; 11:374-87. https://doi.org/10.1007/s11465-016-0388-8
7. Xue BA, Qinhe ZH, Tiantian LI, Ya ZH. Research on the medium breakdown mechanism of powder mixed near dry electrical discharge machining. Journal of Mechanical Engineering. 2012; 48(7):186-92. https://doi.org/10.3901/JME.2012.07.186
8. Bai X, Zhang QH, Yang TY, Zhang JH. Research on material removal rate of powder mixed near dry electrical discharge machining. The International Journal of Advanced Manufacturing Technology. 2013; 68:1757-66. https://doi.org/10.1007/s00170-013-4973-2
9. Bai X, Zhang Q, Zhang J, Kong D, Yang T. Machining efficiency of powder mixed near dry electrical discharge machining based on different material combinations of tool electrode and workpiece electrode. Journal of Manufacturing Processes. 2013; 15(4):474-82. https://doi.org/10.1016/j.jmapro.2013.09.005

10. Wang X, Liu Y, Zhang Y, Sun Q, Li Z, Shen Y. Characteristics of plasma channel in powder-mixed EDM based on monopulse discharge. The International Journal of Advanced Manufacturing Technology. 2016; 82:1063-9. https://doi.org/10.1007/s00170-015-7236-6
11. Kumar M, Datta S, Kumar R. Electro-discharge machining performance of Ti–6Al–4V alloy: studies on parametric effect and phenomenon of electrode wear. Arabian Journal for Science and Engineering. 2019; 44:1553-68. https://doi.org/10.1007/s13369-018-3632-1
12. Öpöz TT, Yaşar H, Ekmekci N, Ekmekci B. Particle migration and surface modification on Ti6Al4V in SiC powder mixed electrical discharge machining. Journal of Manufacturing Processes. 2018; 31:744-58. https://doi.org/10.1016/j.jmapro.2018.01.002
13. Khullar VR, Sharma N, Kishore S, Sharma R. RSM-and NSGA-II-based multiple performance characteristics optimization of EDM parameters for AISI 5160. Arabian Journal for Science and Engineering. 2017; 42(5):1917-28. https://doi.org/10.1007/s13369-016-2399-5
14. Liu JF, Guo YB. Residual stress modeling in electric discharge machining (EDM) by incorporating massive random discharges. Procedia Cirp. 2016; 45:299-302. https://doi.org/10.1016/j.procir.2016.02.060
15. Rao PS, Ramji K, Satyanarayana B. Effect of wire EDM conditions on generation of residual stresses in machining of aluminum 2014 T6 alloy. Alexandria Engineering Journal. 2016; 55(2):1077-84. https://doi.org/10.1016/j.aej.2016.03.014
16. Shabgard M, Seydi S, Seyedzavvar M. Novel approach towards finite element analysis of residual stresses in electrical discharge machining process. The International Journal of Advanced Manufacturing Technology. 2016; 82:1805-14. https://doi.org/10.1007/s00170-015-7510-7
17. Kumar S, Grover S, Walia RS. Effect of hybrid wire EDM conditions on generation of residual stresses in machining of HCHCr D2 tool steel under ultrasonic vibration. International Journal on Interactive Design and Manufacturing (IJIDeM). 2018; 12:1119-37. https://doi.org/10.1007/s12008-018-0474-8
18. Khundrakpam NS, Brar GS, Deepak D, Nanak G. A comparative study on machining performance of wet EDM, near dry EDM and powder mixed near dry EDM. Int J Appl Eng Res. 2018; 13(11):9378-81.
19. Chow HM, Yan BH, Huang FY, Hung JC. Study of added powder in kerosene for the micro-slit machining of titanium alloy using electro-discharge machining. Journal of Materials Processing Technology. 2000; 101(1-3):95-103. https://doi.org/10.1016/S0924-0136(99)00458-6
20. Kumar S, Batra U. Surface modification of die steel materials by EDM method using tungsten powder-mixed dielectric. Journal of Manufacturing Processes. 2012; 14(1):35-40. https://doi.org/10.1016/j.jmapro.2011.09.002
21. Kumar S, Singh R, Batish A, Singh TP, Singh R. Investigating surface properties of cryogenically treated titanium alloys in powder mixed electric discharge machining. Journal of the Brazilian Society of Mechanical Sciences and Engineering. 2017; 39:2635-48. https://doi.org/10.1007/s40430-016-0639-y
22. Sundriyal S, Walia RS. Experimental investigation of the micro-hardness of EN-31 die steel in a powder-mixed near-dry electric discharge machining method. Strojniski Vestnik/Journal of Mechanical Engineering. 2020; 66(3). https://doi.org/10.5545/sv-jme.2019.6474
23. Zhao WS, Meng QG, Wang ZL. The application of research on powder mixed EDM in rough machining. Journal of Materials Processing Technology. 2002; 129(1-3):30-3. https://doi.org/10.1016/S0924-0136(02)00570-8
24. Tripathy S, Tripathy DK. An approach for increasing the micro-hardness in electrical discharge machining by adding conductive powder to the dielectric. Materials Today: Proceedings. 2017; 4(2):1215-24. https://doi.org/10.1016/j.matpr.2017.01.140
25. Furutania K, Saneto A, Takezawa H, Mohri N, Miyake H. Accretion of titanium carbide by electrical discharge machining with powder suspended in working fluid. Precision Engineering. 2001; 25(2):138-44. https://doi.org/10.1016/S0141-6359(00)00068-4
26. Dewangan K, Shukla S. Investigation and Optimization of Wire EDM Process Parameters for Inconel 925 Superalloy Using the Taguchi Gray Relation. International Conference on Sustainable Technologies and Advances in Automation, Aerospace and Robotics. Singapore: Springer Nature Singapore. 2022; 149-62. https://doi.org/10.1007/978-981-99-2349-6_13
27. Singh NK, Balaguru S. Fabrication and mechanical characterization of Al Zn Cu alloy/SiC/TiB2 Hybrid Reinforced Metal Matrix Composite using top loaded bottom pouring stir casting method, Silicon, No. 0123456789; 2023. https://doi.org/10.1007/s12633-023-02648-4
28. Singh NK, Sethuraman B. Development and characterization of Aluminium AA7075 hybrid composite foams (AHCFs) using SiC and TiB2

reinforcement. Int J Met. 2023 https://doi.org/10.1007/s40962-023-01009-6
29. Singh NK, Pradhan SK. Experimental and numerical investigations of pipe orbital welding process. Materials Today: Proceedings. 2020; 27:2964-9. https://doi.org/10.1016/j.matpr.2020.04.902
30. Rathore Rk, Awasthy M, Himte R, Shukla Ak, Kanoje N, Singh Nk. Response Surface Optimized Robotic Spray-Painting Metamodeling for Fanuc Paint Robot P-250ib/15.
31. Singh NK, Balaguru S. Experimental analysis of foaming agent contents in AA7075/SiC closed cell aluminum composite foam. In Sethuraman B, Jain P, Gupta M. (Eds) Recent Advances in Mechanical Engineering. STAAAR 2022. Lecture Notes in Mechanical Engineering. Springer, Singapore. https://doi.org/10.1007/978-981-99-2349-6_51
32. Rathore RK, Singh NK, Xavier JF. Characterization of AA7075 alloy foam using calcium and magnesium carbonate as foaming agents. Processing and Characterization of Materials: Select Proceedings of CPCM 2020. 2021; 289-97. https://doi.org/10.1007/978-981-16-3937-1_30